

Production of cold formaldehyde molecules for study and control of chemical reaction dynamics with hydroxyl radicals

Eric R. Hudson,* Christopher Ticknor, Brian C. Sawyer, Craig A. Taatjes,† H. J. Lewandowski, J. R. Bochinski,‡
J. L. Bohn, and Jun Ye§

JILA, National Institute of Standards and Technology and University of Colorado, Department of Physics, University of Colorado,
Boulder, Colorado 80309-0440, USA

(Received 17 August 2005; revised manuscript received 8 February 2006; published 6 June 2006)

We propose a method for controlling a class of low temperature chemical reactions. Specifically, we show the hydrogen abstraction channel in the reaction of formaldehyde (H_2CO) and the hydroxyl radical (OH) can be controlled through either the molecular state or an external electric field. We also outline experiments for investigating and demonstrating control over this important reaction. To this end, we report the first Stark deceleration of H_2CO . We have decelerated a molecular beam of H_2CO essentially to rest, producing molecules at 100 mK with a density of $\sim 10^6 \text{ cm}^{-3}$.

DOI: [10.1103/PhysRevA.73.063404](https://doi.org/10.1103/PhysRevA.73.063404)

PACS number(s): 32.60.+i, 82.20.-w, 33.80.Ps, 39.10+j

Recent exciting developments in ultracold matter research include the creation of ultracold molecules by magneto-association [1], leading to molecular Bose-Einstein condensation [2]. Despite the rich physics demonstrated in these systems, all are characterized by spherically symmetric interactions whose effect is included through one tunable parameter, namely the s-wave scattering length. By contrast, the permanent electric dipole moment possessed by polar molecules permits long-range and anisotropic interactions and enables new methods for external control in an ultra-cold environment [3]. The electric dipole-dipole interaction (and control over it) gives rise to unique physics and chemistry including collision and chemical reaction dynamics. Lack of spherical symmetry in the interaction causes colliding molecules to be attracted or repelled depending on their relative orientation. Thus, an external electric field, which orients the molecules, will have a profound effect on the molecular interactions [4]. Furthermore, because the transition states of a chemical reaction often involve specific orientations of the molecular dipoles, an external electric field may shift the energy barrier to reaction, making a particular reaction pathway more or less favorable. A Stark decelerator [5–8] producing cold polar molecules with tunable and well-defined translational energy is thus an ideal tool for the study of low (or negative) barrier chemical reactions. We note other experiments utilizing photo-association [9–11], helium buffer gas cooling [12], and billiard ball collisions [13] have succeeded in producing cold polar molecules. Furthermore, the possibility of producing polar molecules through the use of a Feshbach resonance is also very exciting [14,15] because of the ultra-cold temperatures possible.

In this article, we present an outline of the properties and possibilities for control of the low temperature reaction of

OH with H_2CO , followed by a detailed report on the production of cold H_2CO molecules via Stark deceleration, a necessary step in the study of these novel dynamics. Modeling suggests for the first time that chemical reactions and collision cross sections can be altered by orders of magnitude through varying either the molecular state, or external electric field strength. We specifically consider the H-abstraction channel in the reaction of H_2CO and OH : $\text{H}_2\text{CO} + \text{OH} \rightarrow \text{CHO} + \text{H}_2\text{O}$. This reaction not only represents a key component in the combustion of hydrocarbons, but also plays an important role in atmospheric chemistry where it is the primary process responsible for the removal of the pollutant, H_2CO [16–22]. Near room temperature the rate of this reaction is weakly dependent on temperature, suggesting the barrier to the process (if any) is very low [18]. Measurements of the thermal activation energy, E_a , range from $E_a/R = 750$ to -931 K [16–21,23], with the most recent measurement giving a value of -135 K [23]. Here R is the universal gas constant. The most accurate calculations [24] predict the energy of the transition state for the abstraction to lie between -700 and $+60 \text{ K}$ relative to the reactants.

Experimentally, both OH [6–8] and H_2CO (this work) molecules have been produced at low temperatures via Stark deceleration. In the case of spontaneous reaction ($E_a < 0$) [16,18,20,21], by magnetically trapping OH in the presence of a tunable bias electric field and “bombarding” the trap with decelerated H_2CO packets, the $\text{OH-H}_2\text{CO}$ total scattering and reaction rates can be mapped as a function of collision energy and applied electric field. Thus E_a can be measured. If $E_a > 0$, as some measurements and theory suggest [17,19,22,24], the collision energy tuning afforded by the Stark decelerator provides a direct way to measure the energy barrier to reaction. Unlike thermal kinetics studies, which rely on fitting the Arrhenius formula to reaction rates, the Stark decelerator can be used to directly tune the collision energy above and below the threshold energy.

Further motivation for pursuing this particular reaction comes from the prominent position in molecular physics held by H_2CO . As a four-atom asymmetric rotor, H_2CO 's rotational structure and six internal degrees of freedom give rise to the same complexities of much larger molecules. How-

*Electronic address: eric.hudson@Colorado.edu

†Permanent address: JILA VF Combustion Research Facility, Sandia National Laboratories, Livermore, CA 94551-0969.

‡Present address: Department of Physics, NC State University, Raleigh, NC 27695.

§Electronic address: ye@jila.colorado.edu

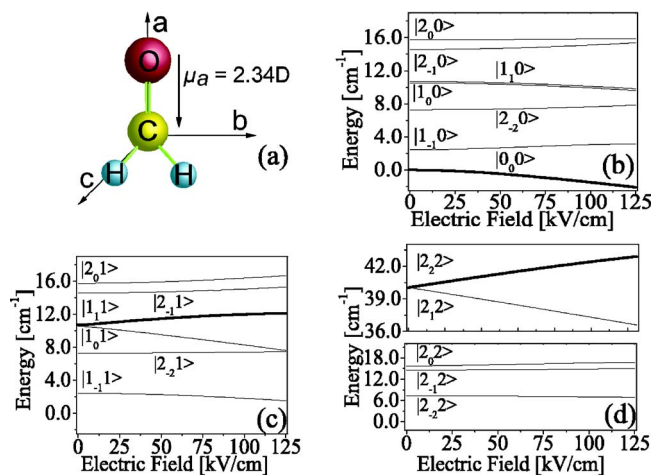


FIG. 1. (Color online) (a) H_2CO . (c) Stark shifts of the low-lying rotational states of H_2CO . States of interest for this work are shown in bold.

ever, as a relatively light molecule, H_2CO is still tractable at a high level of theory, making it an ideal proving ground for molecular physics. Additional incentive for pursuing H_2CO was that until this work an asymmetric rotor had never been decelerated in a Stark decelerator; therefore, this effort opens the door for the production of the most general class of cold molecules.

As shown in Fig. 1(a), H_2CO is a near-symmetric prolate top molecule, with nearly degenerate rotations about the b - and c -axes. The dipole moment, μ_a , along the a -axis causes these nearly degenerate, opposite parity states to experience a large Stark shift with an applied electric field, as shown in Figs. 1(b)–1(d). Here, the states are labeled by their zero-field identity in the $|J, m_J\rangle$ basis, where $\tau = K_a - K_c$ (K_i is the projection of J along the i th axis) [25]. Of particular interest to this work is the $|1_1 1\rangle$ state [Fig. 1(c)], which is the upper component of the lowest J level of ortho-formaldehyde and is hence well populated in our supersonic expansion. This state experiences a large Stark shift (1.32 cm^{-1} at 125 kV/cm), making it excellent for Stark deceleration. There are other states accessible via, for example, stimulated Raman adiabatic passage that offer an improved Stark deceleration efficiency ($|2_2 2\rangle$) or a good candidate for implementing an ac Stark trap ($|0_0 0\rangle$) [26].

The sensitive dependence of cold molecular interactions on internal state and electric field engenders new prospects for probing and controlling chemical reactions. However, a complete theoretical model of the scattering processes is a large task. Nonetheless, simple modeling can suggest the extraordinary influence that can be exerted over the collisions by selecting appropriate initial states, or else by varying an electric field. Much of this control arises from the dipolar interaction itself, as has been stressed in the past [27–29]. We, therefore, construct a scattering model which is realistic with regard to the dipolar interaction, and deliberately schematic with regard to the chemical interaction dynamics. The Hamiltonian, H , used in the scattering calculations takes the following form:

$$H = T + H_{\text{OH}} + H_{\text{H}_2\text{CO}} + H_{\text{Stark}} + H_{dd} + H_{sr} + H_{\text{chem}}. \quad (1)$$

Here T is the kinetic energy, H_{OH} and $H_{\text{H}_2\text{CO}}$ are the Hamiltonians of the separated molecules, and H_{Stark} describes the action of the electric field on the individual molecules. H_{dd} represents the long-range dipole-dipole interaction between the molecules, which depends on the orientations of the molecules relative to the field axis, as well as the distance R between them. This Hamiltonian will be expressed in a basis of molecular eigenstates (including the effect of the field), as was done in Refs. [27,28]. In addition, to prevent the dipole-dipole interaction from overwhelming the short-range interaction, we replace its $1/R^3$ variation with $1/(R^3 + c_{dd})$ for an appropriate constant c_{dd} [30]. The chemical reaction dynamics are modeled in a schematic way by the terms H_{sr} and H_{chem} . The goal of H_{sr} is to mimic an anisotropic interaction with a barrier, not necessarily to characterize the OH- H_2CO system. This approximation is justified for the low reaction barrier where the dipole-dipole interaction dominates over internal molecular dynamics. Thus, we construct a potential as an expansion into Legendre functions,

$$H_{sr} = V_o(R) - 2V_2(R)C_{20}(\theta, \phi). \quad (2)$$

Here (θ, ϕ) represent the spherical angles of the relative coordinate between the molecules, referred to the electric field axis, and C_{20} is a reduced spherical harmonic [31]. The isotropic part of this potential carries the barrier at a radius $R \approx R_b$,

$$V_o(R) = \frac{C_{12}}{R^{12}} - \frac{C_6}{R^6} + D_B \exp\left(\frac{-(R - R_b)^2}{w_b}\right). \quad (3)$$

The height of the barrier depending on D_B is fully adjustable with w_b characterizing its range. In the following, we set the barrier height equal to the threshold energy of the incoming molecule. The resulting isotropic potential has a depth that has arbitrarily been set to 5×10^{-3} atomic units. The radial dependence of V_2 is chosen to have a magnitude comparable to V_o , but to change sign as R crosses R_b , as seen in Fig. 2. This is done to mimic the short-range physics responsible for the chemical reaction as depicted in Fig. 5 and described in the accompanying text. Thus, the polar molecules attract in a head-to-tail configuration for $R > R_b$, but attract in a tail-to-tail configuration upon crossing the barrier. Finally, chemical reactivity (H_{chem}) is modeled by coupling to a purely repulsive artificial channel. The coupling to this channel is represented by a decaying exponential in R , which is of negligible size for $R > R_b$. To complete a chemical reaction, the molecules must cross over the barrier, reverse their relative orientation, and find the artificial channel.

Collision cross sections for OH- H_2CO scattering in this schematic model are shown in Fig. 3. Here both molecules are assumed to be in spin-stretched, weak-field-seeking states: $|Fm_F, \text{parity}\rangle = |22, f\rangle$ for OH, and $|1_1 1\rangle$ for H_2CO . The collision cross sections are plotted as functions of electric field, with the collision energy fixed at 1 mK. The cross section for elastic (spin-changing) collisions is shown as a

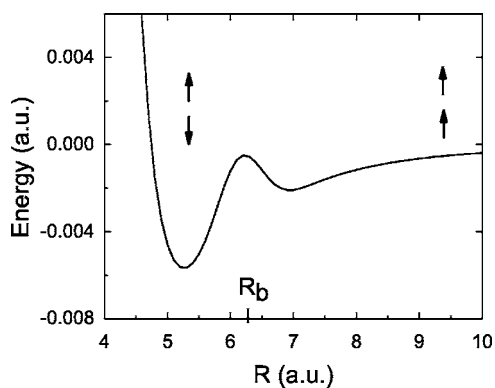


FIG. 2. Schematic lowest-lying adiabatic potential curve for the scattering model. For intermolecular distances $R \gg R_b$, the ordinary dipole-dipole interaction holds, and the molecules attract head-to-tail. As the molecules approach a potential barrier at $R = R_b$, the potential deviates from dipolar behavior, and the sign of V_2 is switched so that, by $R < R_b$, the molecules attract in a tail-to-tail configuration to mimic chemical reaction described below. Also for $R < R_b$, the scattering channel is coupled to an artificial channel (not shown), which represents chemical reactivity.

dashed (solid) line. These cross sections are large and comparable to one another, and exhibit strong modulations as a function of an applied electric field. Modulations of this type have been discussed previously, for the OH-OH scattering system, as arising from purely long-range scattering by the dipole-dipole interaction [27,28]. Thus, these results are relatively robust and independent of the detailed form of the short-range interaction.

The influence of long-ranged dipolar forces should also extend to the chemical reaction dynamics. To illustrate this, we show in Fig. 4 the chemical reaction cross section versus electric field. The collision energy is again assumed to be 1 mK. (Note that, because the reaction mechanism is schematic in our model we report only relative values for the cross sections.) The solid line is for collisions in which both OH and H₂CO molecules are in their strong-field-seeking states. These strong-field seeking states can be easily obtained from Stark decelerated weak-field seeking states by applying microwave field [32]. At this collision energy the field has a profound influence on the reaction cross section, mostly by accessing a large number of resonant states. Considering that each resonant state likely spans a different region of configuration space, mapping out resonances such as these can in principle serve as an extremely sensitive probe to transition states. The dashed trace in Fig. 4 shows the reaction rate for weak-field-seeking states of the reactants. In addition to probing many resonances, this cross section rises by nearly four orders of magnitude as the field increases over a range of 2 kV/cm. This rise is also a direct consequence of the dipole-dipole interaction. In Refs. [27–29], it was shown that polar molecules in weak-field-seeking states scatter at fairly long range at ultra-low energies (of order tens to hundreds of atomic units), owing to avoided crossings in the relevant adiabatic potential energy curves. In other words, the dipole-dipole interaction can “shield” these molecules from ever getting close enough to react chemically. Thus the cross section is strongly suppressed relative to that for

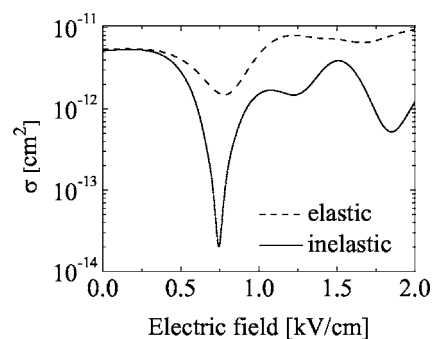


FIG. 3. Elastic (dashed) and spin-changing inelastic (solid) cross sections for cold collisions of spin-stretched OH and H₂CO molecules. These cross sections were computed at a collision energy of 1 mK.

strong-field-seekers. However, as the field is increased, the inner turning point of the relevant potential curve moves to smaller R , making the shielding less effective, and hence, the reaction more likely.

We stress that these results are by no means quantitative predictions of the expected behavior of the OH-H₂CO scattering system. However, they are qualitatively suggestive of the strong dependence of scattering on experimentally accessible parameters such as molecular internal state and applied electric field. Our confidence in these qualitative conclusions is drawn from the fact that they originate largely in the dipolar interaction, which can be treated accurately. More detailed theoretical studies, including more realistic potential energy surfaces, are planned [33].

An important capability for current experiments (not included in our model) is the direct control of the H-abstraction reaction barrier height through the application of an external electric field. The basic H-abstraction reaction mechanism [19] is shown in Fig. 5. We note that Ref. [34] presents a slightly different H-abstraction configuration, but with the same end-to-end dipole coupling scheme. During the H-abstraction process, the energy required to rotate one dipole moment (OH) versus the other (H₂CO) enables our proposed control of reaction dynamics using an external electric field. Hence, the two abstraction configurations present no difference other than the magnitude of the shift we can create in the reaction barrier. The important characteristic to note is that the hydrogen-bonded complex (HBC) in the second panel (Fig. 5) forms along an attractive direction of the two electric dipoles, but in the transition state (TS) the OH dipole has essentially flipped its orientation relative to the H₂CO dipole. While an external electric field, which orients the molecules, would allow (and perhaps even encourage) the formation of the HBC; it would add an energy barrier to the formation of the TS, and thus the H-abstraction channel through the OH dipole-field interaction. Based on the bond geometries shown in Ref. [19], the addition to the energy barrier in going from the HBC to the TS is $\sim 1.8\mu_{\text{OH}}|\vec{E}|$, where μ_{OH} is the expectation value of the OH dipole. For a high, yet attainable, electric field of 250 kV/cm, the additional barrier energy would be 10 K. Assuming a reaction barrier at a H₂CO collision speed of 223 m/s (60 K [24]) the applied electric field would shift the

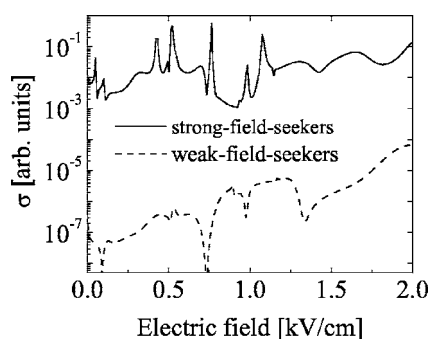


FIG. 4. Calculated chemical reaction cross sections at a collision energy of 1 mK, vs electric field, using the model in the text.

required collision velocity to 234 m/s, well within the Stark decelerator resolution.

The decelerator used for H₂CO is similar to the apparatus in our previously described OH experiments [6,7,35]. Molecules in a skimmed, pulsed supersonic beam are focused by an electrostatic hexapole field to provide transverse coupling into the Stark decelerator. The Stark decelerator is constructed of 143 slowing stages spaced 5.461 mm apart with each stage comprised of two cylindrical electrodes of diameter 3.175 mm separated axially by 5.175 mm and oppositely biased at high voltage (± 12.5 kV). Successive stages are oriented at 90° to each other to provide transverse guiding of the molecular beam. The geometry of the slowing stages provides an electric field maximum between the electrodes with the field decreasing away from the electrode center. Switching the electric field when the molecules are directly between two adjacent stages (no deceleration) is denoted by a synchronous phase angle of $\phi_o = 0^\circ$ (referred to as bunching), while switching the electric field when the molecules are between the electrodes (maximum deceleration, minimum stable area in phase space) is denoted by $\phi_o = 90^\circ$.

The H₂CO molecules are produced from the cracking of

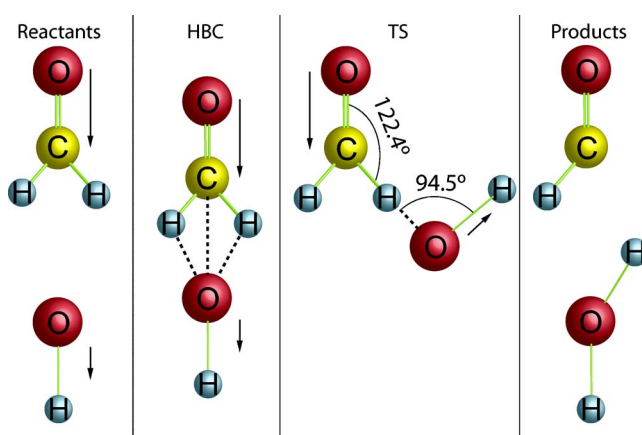


FIG. 5. (Color online) The reaction mechanism for the H-abstraction channel following Ref. [19]. The molecules initially attract in the head-to-tail configuration forming the hydrogen bonded complex (HBC). The chemical reaction proceeds via the transition state (TS) to the final reaction products.

the formaldehyde polymer to produce the monomer, which is passed through a double u-tube apparatus [36]. Xenon at 200 kPa pressure is flowed over the collected H₂CO, held at 196 K where H₂CO has ~ 2.7 kPa vapor pressure. In this work, the Xe-H₂CO mixture was expanded through either a current-loop (60 μ s pulse length) or a solenoid supersonic valve (500 μ s pulse length), producing beams with a mean speed (spread) of 470 m/s (10%) and 350 m/s (10%), respectively. The higher mean speed of the current-loop valve pulse is due to the documented heating effects of these devices [37].

H₂CO is detected using laser-induced fluorescence. The molecules are excited from the $|1,1\rangle$ ground state by photons at 353 nm generated from a frequency-doubled, pulsed-dye laser (PDL) pumped by a Nd:YAG laser to the \tilde{A}^1A electronically excited state with one quantum in the ν_4 out-of-

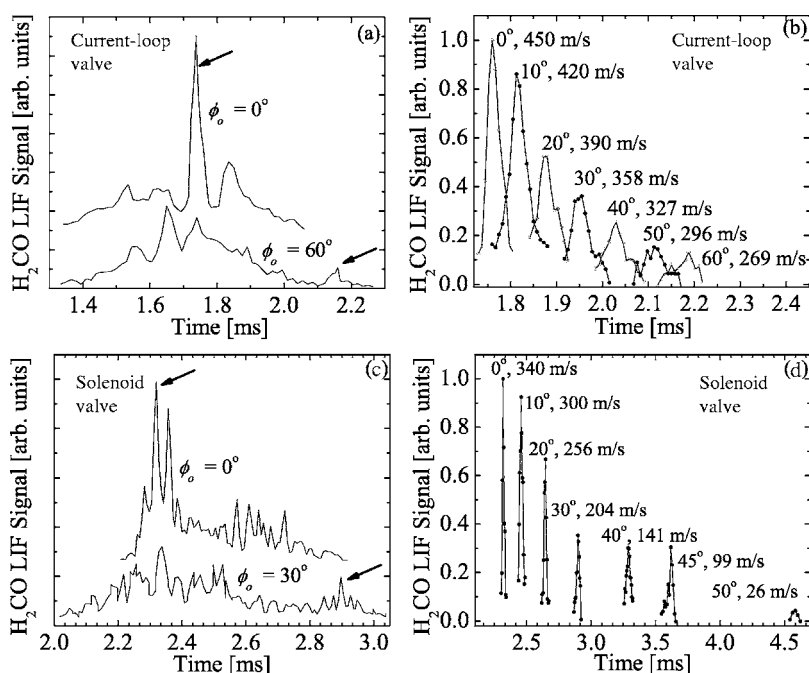


FIG. 6. TOF data for decelerated H₂CO, showing bunching and deceleration off the main pulse (offset down for clarity) for both (a) the current-loop and (c) solenoid valves. Stark decelerated packets of H₂CO at the output of the decelerator for both the (b) current-loop and (d) solenoid valves.

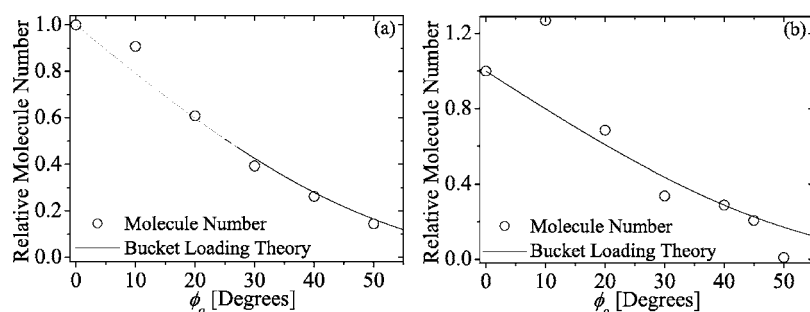


FIG. 7. Comparison of decelerated packet molecule number to the expected for (a) the current-loop valve and (b) the solenoid valve.

plane bending vibrational mode. Approximately 40% of the excited H_2CO decays nonradiatively [38], while the remaining molecules emit distributed fluorescence from 353 to 610 nm [39]. This fluorescence is collected, filtered, and imaged onto a photo-multiplier tube. The output of the photo-multiplier tube is sent to a multi-channel scaler, which serves as a gated photon counter. Operating the decelerator at 5 Hz and the PDL system at 10 Hz allows a “lock-in” type data-collection, such that every other signal is subtracted from the total photon counts. By scanning the delay between the PDL system and the triggering of the valve, a time-of-flight (TOF) curve is generated. A single data point is generated by collecting photon counts for 30–2400 s (depending on the required signal to noise).

Shown in Fig. 6 are TOF measurements taken ~ 1 cm after the exit of the decelerator, which is ~ 0.9 m downstream from the valve. Data taken using the current-loop valve is shown in the top two panels [Figs. 6(a) and 6(b)], while data for the solenoid valve is shown in the bottom two panels [Figs. 6(c) and 6(d)]. In these figures the time axis is relative to the beginning of deceleration. In Fig. 6(a) when the decelerator is operated at $\phi_0 = 0^\circ$, a large peak in the TOF curve denotes the arrival (marked by an arrow) of the phase stable packet whose density is $\sim 10^6 \text{ cm}^{-3}$ and contains a few million molecules. For these molecules no deceleration has occurred [40]. Also shown in Fig. 6(a), but offset for clarity is the TOF curve for deceleration at $\phi_0 = 60^\circ$. Here the arrow denotes the arrival of a slowed, isolated H_2CO packet with a mean velocity of 269 m/s. In this curve the signal of deceleration is unmistakable, a peak in the TOF data arriving later than the main pulse. Displayed in Fig. 6(b) are TOF curves for only the slowed molecular packets as a function of ϕ_0 . The effect of deceleration is evident, as ϕ_0 increases and more energy per stage is removed, the phase stable packets arrive later in time signifying the reduction in velocity. For $\phi_0 \leq 50^\circ$ the phase stable packets have not been decelerated off the main pulse and, therefore, their baseline values differ from that of the higher ϕ_0 .

While the solenoid type valve is much less stable in pulse-to-pulse molecule number than the current-loop valve, it supplies a slower molecular pulse with a mean speed in agreement with a room temperature Xenon expansion. The benefit of the lower initial speed is seen directly in Fig. 6(c), where only $\phi_0 = 30^\circ$ is required to decelerate a packet of molecules such that it arrives after the main pulse. Because of the long pulse from the solenoid valve, the associated TOF structure in Fig. 6(c) is more complicated than that of Fig. 6(a) due to the loading of many buckets at the beginning of the

deceleration sequence. Figure 6(d) further demonstrates the advantage of a lower initial speed, which Fig. 6(b) shows only the decelerated phase stable molecular packets. As in Fig. 6(b) the baseline of the packets varies as they are decelerated off of the main pulse. Here it is seen that with only $\phi_0 = 50^\circ$, the molecular packet is decelerated down to 26 m/s (contrast this with 296 m/s for the current-loop valve). This slowed packet contains a few thousand molecules at a density of $\sim 10^6 \text{ cm}^{-3}$ and a translational temperature of ~ 100 mK as set by the phase space acceptance of the decelerator.

Based on the matching of the molecular phase space at the entrance of the decelerator to the decelerator acceptance, it is possible to predict the molecule number in a given packet. Shown in Figs. 7(a) and 7(b) as open circles are the TOF-deconvolved, integrated molecular numbers for the decelerated packets relative to operation at $\phi_0 = 0^\circ$ for the current-loop valve and solenoid valve, respectively. Also, shown in these figures as solid lines are a simple theory for the dependence of the molecule number in a stable packet on ϕ_0 taken from Eq. (9) of Ref. [35]. The agreement of the theory with the experimental data in Fig. 7(a) is excellent, with the only noticeable deviation at $\phi_0 = 10^\circ$. This is likely because we have neglected any effects due to the transverse phase space, and because $\phi_0 = 10^\circ$ experiences more of the slowing field than $\phi_0 = 0^\circ$ it has a larger transverse acceptance, while the longitudinal acceptances are similar. The molecule number instability of the solenoid valve is responsible for most of the deviations from the expected behavior in Fig. 7(b). For the data point at $\phi_0 = 50^\circ$, however, the low mean speed allows the pulse to expand spatially much more than $\phi_0 = 0^\circ$ to which it is normalized as it exits the decelerator enroute to the detection region. Thus the data point appears below the expected.

To observe the OH- H_2CO collision and reaction dynamics requires monitoring both the OH population and the production of the formyl radical (CHO). The lowest temperature (228 K) measurement [18] of the reaction finds the reaction rate as $10^{-11} \text{ cm}^3 \text{ s}^{-1}$. Since $E_a \sim 0$ the reaction rate at our temperatures of interest will likely be similar. Thus, for a trap volume of 1 cm^3 and reactant densities of 10^6 cm^{-3} we estimate the reaction rate as $10 \text{ molecule s}^{-1}$ and the required signal-to-noise ratio for OH detection at 10^5 . For cold H_2CO at 25 m/s colliding with a 1 cm long magnetic trap of OH this leads to a production rate of CHO as one molecule per 250 pulses. Clearly, observation of this reaction with current conditions would be heroic, however, further improvements such as multiple trap loading and secondary cooling of the

molecular samples, which will increase the sample density, should make these observations possible.

In summary, we have detailed new methods to study interspecies molecular collision and reaction dynamics, and have shown how control of these processes may be achieved. We have also demonstrated experimental preparation of both

cold polar molecules required for these studies.

Funding support for this work comes from DOE, NSF, NIST, and the Keck Foundation. CAT is supported by the Division of Chemical Sciences, Geosciences, and Biosciences, the Office of Basic Energy Sciences, the DOE.

-
- [1] E. A. Donley *et al.*, *Nature (London)* **417**, 529 (2002).
[2] M. Greiner, C. A. Regal, and D. S. Jin, *Nature (London)* **426**, 537 (2003); M. W. Zwierlein, C. A. Stan, C. H. Schunck, S. M. F. Raupach, S. Gupta, Z. Hadzibabac, and W. Ketterle, *Phys. Rev. Lett.* **91**, 250401 (2003); S. Jochim *et al.*, *Science* **302**, 2101 (2003); T. Bourdel, L. Khaykovich, J. Cubizolles, J. Zhang, F. Chevy, M. Teichmann, L. Tarruell, S. J. J. M. F. Kokkelmans, and C. Solomon, *Phys. Rev. Lett.* **93**, 050401 (2003).
[3] Magnetic dipoles and electric quadrupoles also present anisotropic interactions. See A. Griesmaier, J. Werner, S. Hensler, J. Stuhler, and T. Pfau, *Phys. Rev. Lett.* **94**, 160401 (2005); R. Santra and C. H. Greene, *Phys. Rev. A* **67**, 062713 (2003).
[4] A. V. Avdeenkov and J. L. Bohn, *Phys. Rev. A* **66**, 052718 (2002); *Phys. Rev. Lett.* **90**, 043006 (2003).
[5] H. L. Bethlem, G. Berden, and G. Meijer, *Phys. Rev. Lett.* **83**, 1558 (1999).
[6] J. R. Bochinski, E. R. Hudson, H. J. Lewandowski, G. Meijer, and J. Ye, *Phys. Rev. Lett.* **91**, 243001 (2003).
[7] J. R. Bochinski, E. R. Hudson, H. J. Lewandowski, and J. Ye, *Phys. Rev. A* **70**, 043410 (2004).
[8] S. Y. T. van de Meerakker, P. H. M. Smeets, N. Vanhaecke, R. T. Jongma, and G. Meijer, *Phys. Rev. Lett.* **94**, 023004 (2005).
[9] D. Wang, J. Qi, M. F. Stone, O. Nikolayeva, H. Wang, B. Hattaway, S. D. Gensemer, P. L. Gould, E. E. Eyter, and W. C. Stwalley, *Phys. Rev. Lett.* **93**, 243005 (2004).
[10] A. J. Kerman, J. M. Sage, S. Sainis, T. Bergman, and D. Demille, *Phys. Rev. Lett.* **92**, 033004 (2004).
[11] M. W. Mancini, G. D. Telles, A. R. L. Caires, V. S. Bagnato, and L. G. Marcessa, *Phys. Rev. Lett.* **92**, 133203 (2004).
[12] J. D. Weinstein *et al.*, *Nature (London)* **395**, 148 (1998), article SEP 10.
[13] M. S. Elioff, J. J. Valentini, and D. W. Chandler, *Science* **302**, 1940 (2003).
[14] C. Stan, M. W. Zwierlein, C. H. Schunck, S. M. F. Raupach, and W. Ketterle, *Phys. Rev. Lett.* **93**, 143001 (2004).
[15] S. Inouye, J. Goldwin, M. L. Olsen, C. Ticknor, J. L. Bohn, and D. S. Jin, *Phys. Rev. Lett.* **93**, 183201 (2004).
[16] E. D. Morris and H. Niki, *J. Chem. Phys.* **55**, 1991 (1971).
[17] M. R. Soto and M. Page, *J. Phys. Chem.* **94**, 3242 (1990).
[18] L. J. Stief *et al.*, *J. Chem. Phys.* **73**, 2254 (1980).
[19] M. Dupuis and W. A. Lester, *J. Chem. Phys.* **81**, 847 (1984).
[20] H. Niki *et al.*, *J. Chem. Phys.* **88**, 5342 (1984).
[21] R. A. Yetter *et al.*, *J. Chem. Phys.* **91**, 4088 (1989).
[22] H. Y. Li *et al.*, *Chem. Phys.* **307**, 35 (2004).
[23] V. Sivakumaran *et al.*, *Phys. Chem. Chem. Phys.* **5**, 4821 (2003).
[24] B. D'Anna *et al.*, *Phys. Chem. Chem. Phys.* **5**, 1790 (2003).
[25] T. D. Hain, R. M. Moision, and T. J. Curtiss, *J. Chem. Phys.* **111**, 6797 (1999).
[26] J. van Veldhoven, H. L. Bethlem, and G. Meijer, *Phys. Rev. Lett.* **94**, 083001 (2005).
[27] A. V. Avdeenkov and J. L. Bohn, *Phys. Rev. A* **66**, 052718 (2002).
[28] A. V. Avdeenkov and J. L. Bohn, *Phys. Rev. Lett.* **90**, 043006 (2003).
[29] C. Ticknor and J. L. Bohn, *Phys. Rev. A* **71**, 022709 (2005).
[30] B. Kuhn, *J. Chem. Phys.* **111**, 2565 (1999).
[31] D. M. Brink and G. R. Satchler, *Angular Momentum*, 3rd ed. (Clarendon Press, Oxford, 1993).
[32] E. R. Hudson *et al.*, *Phys. Rev. Lett.* **96**, 143004 (2006).
[33] E. R. Meyer and J. L. Bohn (in preparation).
[34] J. R. Alvarez-Idaboy *et al.*, *J. Am. Chem. Soc.* **123**, 2018 (2001).
[35] E. R. Hudson *et al.*, *Eur. Phys. J. D* **31**, 351 (2004).
[36] R. Spence and W. Wild, *J. Chem. Soc.* **1**, 338 (1935).
[37] H. J. Lewandowski *et al.*, *Chem. Phys. Lett.* **395**, 53 (2004).
[38] W. E. Henke *et al.*, *J. Chem. Phys.* **76**, 1327 (1982).
[39] K. Shibuya *et al.*, *J. Phys. Chem.* **83**, 940 (1979).
[40] It is important to note that even though the speed of this packet is 450 m/s, 20 m/s lower than the pulse mean speed, no deceleration has occurred. Instead, the molecules in the pulse whose speed was in the range from 450 m/s \pm 25 m/s were loaded into the phase stable bucket as detailed in our earlier work [34].